Time-domain simulation of damped impacted plates. I. Theory and experiments

Antoine Chaigne and Christophe Lambourg

Citation: The Journal of the Acoustical Society of America **109**, 1422 (2001); doi: 10.1121/1.1354200
View online: https://doi.org/10.1121/1.1354200
View Table of Contents: https://asa.scitation.org/toc/jas/109/4
Published by the Acoustical Society of America

Time-domain simulation of damped impacted plates. I. Theory and experiments

Antoine Chaigne[a] and Christophe Lambourg[b]
Ecole Nationale Supérieure des Télécommunications, Département TSI, CNRS URA 820, 46 Rue Barrault, 75634 Paris Cedex 13, France

(Received 3 December 1999; revised 11 January 2001; accepted 13 January 2001)

A time-domain formulation for the flexural vibrations in damped rectangular isotropic and orthotropic plates is developed, in order to investigate transient excitation of plates by means of sound synthesis. The model includes three basic mechanisms of damping (thermoelasticity, viscoelasticity and radiation) using a general differential operator. The four rigidity factors of the plate are modified by perturbation terms, each term corresponding to one specific damping mechanism. The first damping term is derived from the coupling between the thermoelastic stress–strain relations and the heat diffusion equation. The second term is obtained from the general differential formulation of viscoelasticity. The third term is obtained through a Padé approximation of the damping factor which governs the coupling of the plate with the surrounding air. The decay factors predicted by the model reproduce adequately the dependence on both dimensions and frequency of the decay factors measured on rectangular plates of various sizes and thicknesses made of four different materials (aluminum, glass, carbon fiber, and wood). The numerical resolution of the complete problem, including initial and boundary conditions, and the comparison between real and simulated sounds are presented in a companion paper [J. Acoust. Soc. Am. **109**, 1433–1447 (2000)]. [DOI: 10.1121/1.1354200]

PACS numbers: 43.40.Dx [CBB]

I. INTRODUCTION

A noticeable part of our daily acoustic environment is made of transient sounds radiated by vibrating structures. These sounds may have pleasant qualities, like those produced by stringed and percussive musical instruments, for example. On the contrary, most of the sounds produced by impacts will likely be considered as undesirable noise.[1,2]

A frequency approach is generally not sufficient for understanding the complexity of transients, since most of the auditory information is often included in the short initial part of the sound. Therefore, a time-domain approach seems more appealing. Another meaningful and attractive aspect of this approach is that the sound resulting from time-domain modeling can be used for musical purposes, in the context of sound synthesis, and for the constitution of systematic series of stimuli for psychoacoustical tests where the goal is to investigate the relationships between physical parameters of structures and subjective judgments.

The geometry of real vibrating structures are often very complex, and it is not always conceivable to model them with great accuracy. However, one efficient strategy consists of approximating structures of complex shapes by structures of simpler geometry, such as plates and shells, in order to grasp the most essential features of the vibratory and acoustical problems. To a first approximation, some properties of panels and of some stringed musical instruments such as the guitar, for example, can be reasonably understood by studying the vibroacoustical behavior of thin plates. The interest in plates is reflected in the considerable amount of reliable results and models published on these structures.

From an auditory point of view, the quality of impacts, and of musical percussive sounds, is highly correlated to the frequency-dependent decay times of the excited eigenfrequencies. A consequence of the dependence on frequency of the decay times is that the power spectrum of the sounds varies with time. The decay times are due to the various mechanisms of loss in the materials. These mechanisms are not identical for all materials: metallic plates will be subjected to thermoelastic damping, whereas viscoelasticity will be one major cause for the attenuation of sound in materials such as glass and carbon fibers, for example. As a consequence, there is a strong need for developing accurate models of these kinds of damping in order to reproduce convincingly the sounds generated by a large variety of materials.

In order to address some of the problems presented above with the help of simulations, a time-domain numerical model of damped isotropic and orthotropic plates excited by an impact has been developed. Previous work by the authors on the comparison between numerical simulations and experiments for an undamped impacted isotropic plate has shown the efficiency of the method.[3]

The paper is organized as follows. In Sec. II the conditions under which three fundamental mechanisms of damping in plates (thermoelasticity, viscoelasticity and radiation) can be expressed by means of a general differential operator are shown. The influence of each of these three mechanisms on the decay times of the eigenfrequencies of the plate is presented. In Sec. III, the procedure for measuring accurately the eigenfrequencies and decay times of the free vibrations, for freely suspended plates, is presented. From these mea-

[a]Present address: ENSTA-UME, Chemin de la Hunière 91761 Palaiseau cedex, France; electronic mail: chaigne@ensta.fr
[b]Present address: 64 rue des Moines, 75017 Paris, France.

surements, the values of the rigidity constants and of the damping constants are derived for four different isotropic and orthotropic materials (aluminum, glass, carbon fibers and wood) which illustrate various combinations of damping mechanisms. For each plate material, the dependence with frequency of the decay factors predicted by the model is compared to measurements. The presentation of the complete model, including initial impact by a mallet and boundary conditions, the numerical resolution of the problem, and the comparison between real and simulated sounds is made in a companion paper.[4]

II. THEORY

This section starts with a short review of the undamped plate equations. This review is followed by the successive presentation of the three mechanisms of damping under study: thermoelasticity, viscoelasticity, and radiation. It is shown, in particular, how the rigidity coefficients of the plate can be modified in order to account for each of these mechanisms. The section ends with the summary of the damped plate equations used in the simulations. The equations are generally written in the orthotropic case. In some situations, however, the simplified equations, which are valid in the isotropic case only, are highlighted.

A. The undamped orthotropic plate equations

In Cartesian coordinates, the free flexural vibrations of an orthotropic Kirchhoff–Love plate of thickness h, with symmetry axes of the material parallel to the sides of the plate in the (x,y) plane, are governed by the following equations:[5,6]

$$\begin{pmatrix} M_x(x,y) \\ M_y(x,y) \\ M_{xy}(x,y) \end{pmatrix} = -h^3 \begin{pmatrix} D_1 & D_2/2 & 0 \\ D_2/2 & D_3 & 0 \\ 0 & 0 & D_4/2 \end{pmatrix} \begin{pmatrix} W_{,xx}(x,y) \\ W_{,yy}(x,y) \\ W_{,xy}(x,y) \end{pmatrix},$$

$$\rho h s^2 W(x,y) = M_{x,xx}(x,y) + M_{y,yy}(x,y) + 2M_{xy,xy}(x,y), \quad (1)$$

where $W(x,y,t)$ is the vertical transverse displacement. The subscripts $,xx$, $,yy$ and $,xy$ denote the partial derivatives. $M_x(x,y)$, $M_y(x,y)$ and $M_{xy}(x,y)$ are the bending and twisting moments, ρ is the density and D_i are the four rigidity constants of the plate. For convenience, the equations are written in the Laplace domain. As a consequence, a partial derivative versus time $\partial/\partial t$ is replaced by a multiplication by s, where s is the Laplace variable. This rule is used throughout this paper.

B. Thermoelasticity

Thermoelastic damping can affect the vibrations in plates with significant thermal conductivity, such as metallic plates. A model for this damping can be derived from the equations that govern the coupling between plate vibrations and the diffusion of heat.[7,8] In the present paper, the method previously used by Cremer for isotropic bars is extended to orthotropic plates, in order to derive the expressions for the complex rigidity constants.[9]

The temperature change θ is assumed to be sufficiently small so that the stress–strain relationships can be linearized. Therefore, we get the stress components:

$$\begin{aligned} \sigma_{xx} &= -12z\left(D_1 W_{,xx} + \frac{D_2}{2} W_{,yy}\right) - \phi_x \theta, \\ \sigma_{yy} &= -12z\left(D_3 W_{,yy} + \frac{D_2}{2} W_{,xx}\right) - \phi_y \theta, \\ \sigma_{xy} &= -6zD_4 W_{,xy}, \end{aligned} \quad (2)$$

where ϕ_x and ϕ_y are the thermal coefficients of the material. In the particular case of an isotropic material, we have $\phi_x = \phi_y = \phi$. Equation (2) has to be complemented by the heat diffusion equation, assuming that θ only depends on z:

$$\kappa \theta_{,zz} - \rho C s \theta = -zT_0 s(\phi_x W_{,xx} + \phi_y W_{,yy}), \quad (3)$$

where T_0 is the absolute temperature, C is the specific heat at constant strain, and κ is the thermal conductivity. Following the method used by Cremer,[9] it is assumed that $\theta(z)$ is given by an equation of the form:

$$\theta(z) = \theta_0 \sin\frac{\pi z}{h} \quad \text{for } z \in \left[-\frac{h}{2}, \frac{h}{2}\right], \quad (4)$$

which takes into account the fact that there is no heat transmission between plate and air. Through integration of $z\sigma_{ij}$ over the thickness h of the plate, one obtains, in the Laplace domain, the relationship between the bending and twisting moments M_{ij} and the partial derivatives of the transverse displacement W of the plate. It is found, finally, that the rigidity factors are now complex functions of the form:

$$\begin{aligned} \tilde{D}_1(s) &= D_1 + \phi_x^2 \frac{s\zeta}{1+\tau s}, \\ \tilde{D}_2(s) &= D_2 + 2\phi_x \phi_y \frac{s\zeta}{1+\tau s}, \\ \tilde{D}_3(s) &= D_3 + \phi_y^2 \frac{s\zeta}{1+\tau s}, \\ \tilde{D}_4(s) &= D_4, \end{aligned} \quad (5)$$

where the thermoelastic relaxation time τ and the thermal constant ζ are given by:

$$\tau = \frac{\rho C h^2}{\kappa \pi^2} \quad \text{and} \quad \zeta = \frac{8T_0 h^2}{\kappa \pi^6}. \quad (6)$$

As a consequence of Eq. (6), the thermoelastic losses decrease as the thickness h of the plate increases. Notice also that D_4 is real. As a consequence, the particular flexural modes of the plate, such as the torsional modes, for example, which involve this rigidity factor will be relatively less affected by thermoelastic damping than the other modes. In other words, the thermoelastic damping factors depend on the modal shapes. These important features of thermoelastic damping will be confirmed by measurements of the decay times in aluminum plates of various sizes (see Sec. III). In what follows, the complex rigidities are written in the form:

$$\tilde{D}_i(s)=D_i[1+\tilde{d}_{it}(s)]=D_i\left[1+\frac{sR_i}{s+c_1/h^2}\right],\quad i=[1,2,3],$$
$$\tilde{D}_4(s)=D_4. \tag{7}$$

In practice, due to the order of magnitude for the thermal constants of usual materials, the $\tilde{d}_{it}(s)$ can be considered as perturbation terms of the complex rigidities, due to thermoelasticity. For convenience, these terms are written in Eq. (7) using the following nondimensional numbers:

$$R_1=\frac{8T_0\phi_x^2}{\pi^4 D_1\rho C};\quad R_2=\frac{16T_0\phi_x\phi_y}{\pi^4 D_3\rho C};\quad R_3=\frac{8T_0\phi_y^2}{\pi^4 D_3\rho C}. \tag{8}$$

In addition, the decay factor $1/\tau$ is written here in the form c_1/h^2 in order to highlight the fact that this factor is proportional to the inverse squared thickness of the plate.

C. Viscoelasticity

A large class of materials is subjected to viscoelastic damping.[10] This is the case for three of the four materials investigated in this study: glass, carbon fiber and wood. A convenient method for representing the viscoelastic phenomena in a material is to use a differential formulation between stress (σ) and strain (ε) tensors of the form:[11]

$$\sigma+\sum_{w=1}^{N} q_w\frac{\partial^w\sigma}{\partial t^w}=E\left[\varepsilon+\sum_{v=1}^{N} q_v\frac{\partial^v\varepsilon}{\partial t^v}\right]. \tag{9}$$

As a consequence, the differential equations involving the flexural displacements and moments in thin plates contain time derivatives up to order N. By taking the Laplace transform of both sides in Eq. (1), one can define the complex rigidities due to viscoelasticity:

$$\tilde{D}_i(s)=D_i(1+\tilde{d}_{iv}(s))=D_i\frac{1+\sum_{v=1}^{N}s^v p_{iv}}{1+\sum_{w=1}^{N}s^w q_w}. \tag{10}$$

Equation (10) is a particular class of representation for the complex rigidities. This operator is bounded under the condition:[12]

$$q_N\neq 0. \tag{11}$$

Another restrictive condition on the coefficients in Eq. (10) follows from the fact that the energy for deforming the material from its initial undisturbed state must be positive. In other words, this means that the model must be a so-called ''dissipative'' model.[13] For a generalized viscoelastic strain–stress relationship the Laplace transform of which is given by:

$$\tilde{\sigma}_{ij}=\sum_{k,l}\tilde{a}_{ijkl}(s)\tilde{\epsilon}_{kl}. \tag{12}$$

Gurtin and Sternberg[12] have proved that one necessary condition for the model to be dissipative is:

$$\Im m(X_{ij}\tilde{a}_{ijkl}(j\omega)X_{kl})\geqslant 0\quad\text{for}\quad\omega\geqslant 0 \tag{13}$$

for any real symmetric tensor X_{ij}. For our viscoelastic plate model, Eq. (13) together with Eq. (10) yield the following conditions:

$$p_{1N}>0,\quad p_{3N}>0,\quad p_{4N}>0,$$
$$p_{1N}p_{3N}-\frac{D_2p_{2N}^2}{4D_1D_3}>0. \tag{14}$$

In our method, a so-called Wiechert model (also called generalized Maxwell model) is used. It is a convenient formulation of Eq. (10) which fulfills the conditions (14) and ensures that the model is dissipative.[14] This model is written:

$$\tilde{d}_{iv}(s)=\sum_{n=1}^{N}\frac{sR_{in}}{s+s_n}. \tag{15}$$

As for thermoelastic damping, the viscoelastic losses in the materials considered here are relatively small and thus, the corresponding terms can be viewed as first-order correction terms of the rigidity terms.

One property of Eq. (15) is that the loss factor tends to zero as ω tends to zero. Therefore, in order to account for the fact that experimental decay factors usually tend to a constant (positive) value as ω vanishes, it is necessary to introduce, in addition, an arbitrary viscous damping term proportional to velocity $-R_f(\partial w/\partial t)$ in the bending wave equation [Eq. (1)]. The values obtained for R_f are the result of least-square fit procedures performed on the measured decay factors (see Sec. III). It has been found that introducing this term reduces significantly the number N of factors in the viscoelastic model, for a given degree of accuracy between the model and the experimental data. In practice, it turns out that, for the presently investigated materials, and for the accuracy required, the number N of factors in Eq. (15) remains less than or equal to 2.

D. Damping due to radiation (isotropic plates)

The interaction of vibrating plates with the surrounding air is a fundamental problem in vibroacoustics.[15–17] In this section, the goal is to develop an approximate model in the time-domain which takes into account the effect of radiation on the temporal decay of the free bending vibrations for isotropic plates.

The leading idea is to derive a differential operator for the radiation losses (i.e., a polynomial formulation in the Laplace domain), similar to the one presented in the previous sections for thermoelastic and viscoelastic damping. This should allow us to group all three mechanisms of damping for the free vibrations of plates into a single unified formulation.

The experiments described here, where the plates are freely suspended by light threads, show that in the ''low-frequency'' domain (i.e., below the critical frequency), viscoelastic and/or thermoelastic losses are the main causes of damping (see Sec. III for the four materials under investigation). In this particular situation, there is no damping due to coupling at the boundaries. Above the critical frequency, the damping is mainly governed by radiation for low dissipative materials, such as aluminum and glass. In what follows, it is assumed that the radiation losses become relevant when the wavelength is significantly lower than the dimensions of the plate. Therefore, an asymptotic infinite plate model is used, which simplifies substantially the formulation of the radia-

tion damping. In what follows, no attempt is made to model accurately the mode-by-mode radiation of the finite plate below the critical frequency.

The equations governing the flexural motion of an infinite isotropic plate surrounded by air are the following:[18]

$$\rho h \frac{\partial^2 W(x,y,t)}{\partial t^2} + h^3 D\left(\frac{\partial^4}{\partial x^4} + 2\frac{\partial^4}{\partial x^2 \partial y^2} + \frac{\partial^4}{\partial y^4} \right) W(x,y,t) = f_z(x,y,t) + p(x,y,0-,t) - p(x,y,0+,t), \tag{16}$$

$$\left. \frac{\partial p}{\partial z} \right|_{z=0+} = -\rho_a \frac{\partial^2 W}{\partial t^2}, \tag{17}$$

$$\Delta p - \frac{1}{c^2}\frac{\partial^2 p}{\partial t^2} = 0, \quad \text{for } z>0 \text{ and } z<0, \tag{18}$$

where $D=D_1=D_3=(D_2+D_4)/2$. For a traveling wave of the form $W(x,y)\exp j(\tilde{\omega}t-\underline{k}.\underline{x})$ where k is the wave number and $\tilde{\omega}=\omega+j\alpha_r$ the complex frequency, one can derive from Eqs. (16)–(18) the dispersion equation for the fluid-loaded plate:[18]

$$-\tilde{\omega}^2\left(1+\frac{2\rho_a}{\rho h}\frac{1}{\sqrt{k^2-\frac{\tilde{\omega}^2}{c^2}}} \right) + \frac{Dh^2}{\rho}k^4 = 0. \tag{19}$$

Under the assumption of a light fluid, one can equivalently derive the radiation decay factor α_r from Eq. (19) by reformulating this equation through introduction of a rigidity modulus $\tilde{D}$ of the form:

$$\tilde{D} \simeq D\left(1-\frac{2\rho_a c}{\omega_c \rho h}\frac{1}{\sqrt{\Omega-\Omega^2}} \right), \tag{20}$$

with

$$\omega_c = c^2\sqrt{\frac{\rho}{h^2 D}} \quad \text{and} \quad \Omega = \frac{\omega}{\omega_c}. \tag{21}$$

Now, in order to find an appropriate form for Eq. (20), the complex rigidity $\tilde{D}$ is rewritten in the form of a third order Padé development. The optimization procedure is performed for $s=j\omega$ in the audio range. In the time domain, this yields:

$$\tilde{D}(s) \hat{=} D\left(1+\frac{2\rho_a c}{\omega_c \rho h}\frac{\Sigma_{m=1}^{3} b_m (s/\omega_c)^m}{\Sigma_{n=0}^{3} a_n (s/\omega_c)^n} \right) = D(1+\tilde{d}_r(s)), \tag{22}$$

with $a_0=1.1669$, $a_1=1.6574$, $a_2=1.5528$, $a_3=1$, $b_1=0.0620$, $b_2=0.5950$, $b_3=1.0272$. For orthotropic plates, it is known that Eq. (19) depends on the direction of propagation of the flexural wave in the plate. As a consequence, it was not possible to formulate the radiation damping in the time-domain using an approximation similar to Eq. (22). Therefore, the two examples below which show a relevant contribution of radiation losses in the decay factors, will be limited to isotropic materials: glass and aluminum. For the two examples of orthotropic materials (wood and carbon fiber) presented in Sec. III, the radiation losses are generally masked by the relatively high internal (viscoelastic) losses. In these cases, the discussion on the radiation damping will be restricted to limiting situations, for waves propagating along the axes of symmetry of the material.

E. Summary of the damping model

It is assumed that the three previously examined physical mechanisms of damping are uncorrelated. It is also assumed that the perturbation term $\tilde{d}_i(s)$, for each complex rigidity, is given by the sum of three perturbation terms, each of them corresponding to one specific mechanism. Therefore, in the most general case, the four complex rigidities in our model are given by:

$$\tilde{D}_i(s) = D_i(1+\tilde{d}_i(s)) = D_i(1+\tilde{d}_{it}(s)+\tilde{d}_{iv}(s)+\tilde{d}_r(s)), \quad i=1,..,4, \tag{23}$$

where $\tilde{d}_{it}$ refers to thermoelastic damping, $\tilde{d}_{iv}$ refers to viscoelastic damping and $\tilde{d}_r$ refers to radiation damping. It is clear that the relative contribution of each perturbation term in the measured global damping varies with the material. In some specific cases, one or two terms will become negligible, as will be shown in Sec. III.

In summary, the system of equations used in our model for simulating damped plates is similar in form to Eq. (1), except that each rigidity constant D_i is now replaced by a complex rigidity $\tilde{D}_i(s)$, which represents a differential operator. In addition, a viscous damping term with constant R_f is inserted in the bending wave equation:

$$\begin{pmatrix} \tilde{M}_x(x,y,s) \\ \tilde{M}_y(x,y,s) \\ \tilde{M}_{xy}(x,y,s) \end{pmatrix} = -h^3 \begin{pmatrix} \tilde{D}_1(s) & \tilde{D}_2(s)/2 & 0 \\ \tilde{D}_2(s)/2 & \tilde{D}_3(s) & 0 \\ 0 & 0 & \tilde{D}_4(s)/2 \end{pmatrix} \times \begin{pmatrix} \tilde{W}_{,xx}(x,y,s) \\ \tilde{W}_{,yy}(x,y,s) \\ \tilde{W}_{,xy}(x,y,s) \end{pmatrix},$$

$$\rho h(s^2+R_f s)\tilde{W}(x,y,s) = \tilde{M}_{x,xx}(x,y,s) + \tilde{M}_{y,yy}(x,y,s) + 2\tilde{M}_{xy,xy}(x,y,s) + \tilde{f}_z(x,y,s). \tag{24}$$

In Eq. (24), $\tilde{f}_z(x,y,s)$ represents the source term due to impact which is presented with more details in the companion paper.[4]

III. MEASUREMENTS

A. Experimental set-up

Measurements of eigenfrequencies and decay times are performed on rectangular plates in an anechoic room. The plates are suspended vertically by means of a nylon thread in order to avoid transmission losses. In a first series of experiments, the plate is set into vibration by means of an impact hammer. An FFT (fast Fourier transform) frequency analysis is then performed, with a B&K 2032 frequency analyzer, on the pressure signal recorded at a distance of approximately 1 m from the plate. This analysis yields a first estimate for the eigenfrequencies of the freely vibrating plate.

In a second series of experiments, the plate is acoustically excited by means of a loudspeaker driven by a Philips PM 5193 programmable frequency synthesizer. The frequency of the synthesizer is initially set equal to one of the previously estimated eigenfrequencies of the plate. The transverse velocity of one arbitrary point on the plate is measured by means of a Polytec OFV 2600-352 laser vibrometer. This procedure ensures noncontact excitation and measurements. The frequency is adjusted until the magnitude of the plate velocity reaches its maximum. This yields an accurate estimation of the eigenfrequency. The acoustic source is then suddenly turned off, and the velocity signal delivered by the vibrometer is recorded on a DAT tape. This signal is analyzed using the matrix pencil method.[19] In this parametric method, the signal is assumed to be composed of a finite sum of exponentially decaying sinusoids, whose frequencies, decay times, magnitude, and phases are estimated. In our case, this signal processing technique yields the decay times of the successive eigenfrequencies of the plate with great accuracy.

In case of high damping, the acoustic power of the sound source is not sufficient for exciting flexural vibrations in the plate with enough magnitude. This is the case, for example, in this study for both the carbon fiber and wooden plates, for frequencies above 500 Hz. In this frequency range, an impact hammer excitation had to be used.

B. Link between measured decay times and the damping model

Within the framework of the model, and with the assumption of ''small damping,'' the four loss factors η_i predicted by the model are given by:[20]

$$\eta_i(\omega) \simeq \Im m(\tilde{D}_i(j\omega))/D_i = \Im m(\tilde{d}_i(j\omega)), \quad i=1,..,4. \tag{25}$$

Notice that in Eq. (25) the loss factors are frequency-dependent. As mentioned above, the available measured quantities, for each plate, are the eigenfrequencies ω_p and the decay factors α_p. These decay factors are the inverse of the decay times τ_p, which are measured as the plate vibrates freely with frequency ω_p. The link between the measured α_p and the loss factors defined in Eq. (25) are now examined. The simple case of proportional damping is discussed first.

In a limited number of cases, it is justified to make the assumption of proportional damping.[21] With the additional assumption of small damping, it can be shown that the loss factors and the decay factors, for a given mode p are linked by the expression:[22]

$$\alpha_p(\omega_p) = \frac{\omega_p}{2}\,\eta(\omega_p). \tag{26}$$

This is the case, for example, for glass plates (see below).

In the general case, however, this assumption of proportional damping is too restrictive and does not account for the observed complicated frequency dependence of the decay factors. In this case, it can be shown that the decay factors, for an orthotropic plate, are given by:[20]

$$\alpha_p(\omega_p) = \sum_{i=1}^{4} \frac{\omega_p}{2}\,\eta_i(\omega_p) J_{i,p} \tag{27}$$

with

$$J_{i,p} = \frac{a_i(u_p,u_p)}{\omega_p^2 \|u_p\|^2}, \tag{28}$$

where u_p is the eigenvector of mode p in the undamped case, and where the scalar products $a_i(u_p,u_p)$ are defined by:[20]

$$\begin{aligned}
a_1(u_p,u_p) &= \int_S h^3 D_1 \left(\frac{\partial^2 u_p}{\partial x^2}\right)^2 dS,\\
a_2(u_p,u_p) &= \int_S h^3 D_2 \frac{\partial^2 u_p}{\partial x^2}\frac{\partial^2 u_p}{\partial y^2} dS,\\
a_3(u_p,u_p) &= \int_S h^3 D_3 \left(\frac{\partial^2 u_p}{\partial y^2}\right)^2 dS,\\
a_4(u_p,u_p) &= \int_S h^3 D_4 \left(\frac{\partial^2 u_p}{\partial x \partial y}\right)^2 dS.
\end{aligned} \tag{29}$$

In Eqs. (29), S is the surface of the plate of thickness h and density ρ and $\|u_p\|^2$ is the norm defined as:

$$\|u_p\|^2 = \omega^2 \int_S \rho h u_p^2\, dS. \tag{30}$$

In the isotropic case, Eq. (27) reduces to

$$\alpha_p(\omega_p) = \frac{\omega_p}{2}[\,\eta_1(\omega_p) I_{1,p} + \eta_4(\omega_p) I_{4,p}], \tag{31}$$

where

$$I_{1,p} = J_{1,p} + J_{3,p} + \frac{2D_1}{D_2} J_{2,p} \quad \text{and} \quad I_{4,p} = J_{4,p} - \frac{D_4}{D_1} J_{2,p}. \tag{32}$$

C. Determination of the rigidity constants

1. First estimates of the rigidities

The method used here is largely inspired by the work of McIntyre and Woodhouse.[20] Using Rayleigh's method with polynomial functions as trial functions, a first estimate for the rigidity factor D_4 is obtained from measurement of the first torsional (or twisting) mode f_{11}:

$$D_4 = f_{11}^2 \frac{4\pi^2}{144} \rho \frac{(l_x l_y)^2}{h^2}. \tag{33}$$

The rigidity constants D_1 and D_3 are estimated from measurements of the first flexural modes f_2 and f_3 in the x and y directions, respectively. Assuming that these modes can be approximately predicted from the free–free bar equations, we get:[20]

$$D_1 \simeq 0.0789 \frac{\rho f_2^2 l_x^4}{h^2} \quad \text{and} \quad D_3 \simeq 0.0789 \frac{\rho f_3^2 l_y^4}{h^2}. \tag{34}$$

Finally, a first estimate for D_2 is obtained by considering that, for orthotropic plates, we have the relation:

$$D_2 = 2\sqrt{\nu_{xy}\nu_{yx} D_1 D_3}. \tag{35}$$

Setting the product $\nu_{xy}\nu_{yx}$ to an arbitrary, though realistic, value of 0.01, we get $D_2 \simeq 0.2\sqrt{D_1 D_3}$ as a starting value. In the isotropic case, we simply have:

$$D_1 = D_3 \quad \text{and} \quad D_2 = 2D_1 - D_4. \tag{36}$$

2. Accurate calculation of the rigidity constants

The next step consists of calculating the eigenfrequencies ω_p of the plate from the first estimates of the rigidity constants D_i. This calculation is made by means of the classical Rayleigh–Ritz method, using polynomial trial functions.[21] The procedure is typically applied to the lowest 20 modes of the plate. Correcting terms ΔD_i are then obtained using a first-order approximation:

$$\Delta\omega_p^2 = \sum_{i=1}^{4} \frac{\partial(\omega_p^2)}{\partial D_i}\Delta D_i \quad \text{with} \quad \frac{\partial(\omega_p^2)}{\partial D_i} = J_{i,p}\frac{\omega_p^2}{D_i}, \tag{37}$$

where the $\Delta\omega_p^2$ are the differences between the measured and calculated squared frequencies. The procedure is iterated until the $\Delta\omega_p^2$ are less than a fixed accuracy limit. In practice, a maximum of 3 iterations is necessary for the required accuracy in audio applications (the order of magnitude fixed here is about 1%).

D. Examples of results on four different materials

In order to illustrate the relevance of the above-presented model of damping, the eigenfrequencies and decay times of the free vibrations for rectangular plates made of four different materials are measured and compared to the predictions of the model. For each material, the contributions are specific. For the aluminum plate, it turns out that the damping is mainly governed by thermoelastic and radiation mechanisms. For the three other plates, the damping is due to viscoelasticity and radiation. In the thermoelastic and radiation cases, the damping parameters in Eqs. (7) and (22), respectively, can be compared to predictions based on the physical properties of the material. In the viscoelastic case, there is no similar theoretical background: the model and the damping constants are the results of a least-square fit performed on the experimental data. From the observation of the results obtained for the frequency-dependent decay factors, which generally highlight the most relevant damping mechanisms for each material, damping models are built, with the help of standard optimization procedures, and are tested against the experimental data. In the figures, the experimental points are indicated by ''○,'' whereas the theoretical points are indicated by ''×.'' In some cases (radiation, viscoelasticity for the glass plate), the theoretical model is represented by a solid line.

1. Aluminum

Measurements were conducted on two different plates (see Table I). The first 30 modes were measured by means of acoustic excitation and optical measurement, with the help of a laser vibrometer, in an anechoic room, following the previously described procedure.

Figures 1(a) and (b) show the decay factors (in s^{-1}) as a function of frequency between 0 and 2 kHz, for plates a_1 and a_3, respectively. These figures show that the frequency dependence of the decay factors is far from being monotonic, but rather show an apparently random distribution of values, however with a general tendency to increase with frequency. This apparent randomness is more pronounced for the thinner plate a_1 than for the thicker one a_3. In addition, it can be seen that the mean value of the decay factor is about four times greater for plate a_1 than for plate a_3. This is an indication that the damping in this frequency range might be due to thermoelasticity, see Sec. II, since the decay factors vary as the inverse of squared thickness.

Figures 1(c) and (d) show the variation of the decay factors with frequency, up to 12 kHz, for the same two plates. These figures show clearly that the damping increases strongly above 6 kHz (for the thin plate a_1), and above 3 kHz (for the thick plate a_3), which correspond to the critical frequencies for these two plates. The solid lines superimposed on the experimental points are obtained from the asymptotic model of radiation for isotropic plates developed in Sec. II. This comparison shows that, for these metallic plates, the radiation clearly becomes the dominant damping mechanism above the critical frequency. In Figs. 1(a) and (b) it can be seen that, in the frequency range where thermoelasticity damping is the main cause of damping, the radiation model is significantly lower than the measured decay factors and, consequently, will not affect the prediction of damping in this range.

In order to build a model for these plates, the rigidity constants D_1 and D_4 are derived from the measurements of the 20 first modes, using the method described above. The iteration process is repeated until the average relative frequency error between measurements and simulations is less than 0.5%. The values obtained for D_1 and D_4 are listed in Table I.

For the damping model, in view of the previously described measurements, it is assumed that the perturbation terms in the complex rigidities are only due to thermoelasticity and to radiation. As mentioned in Sec. II, the thermoelastic term only affects $\tilde{D}_1$. Therefore, we write:

$$\tilde{d}_1(s) = \tilde{d}_{1t}(s) + \tilde{d}_r(s) \quad \text{and} \quad \tilde{d}_4(s) = \tilde{d}_r(s). \tag{38}$$

As mentioned in Sec. II, a viscous damping term with constant R_f is added to the bending wave equation, in order to account for the finite damping near the zero frequency. Finally, from Eq. (38), the following decay factors, for each mode p, are derived:

$$\alpha_p = \frac{\omega_p}{2}\Im m(\tilde{d}_{1t}(j\omega_p)I_{1,p} + \tilde{d}_r(j\omega_p)) + \frac{R_f}{2}. \tag{39}$$

Figures 1(a)–(d) show the agreement between the measured decay factors and the simulations obtained with the damping parameters shown in Table I. It is found, in particular, that the thermoelastic constants derived from least-square optimization procedures are of the same order of magnitude as the general constants found in the literature for aluminum. For frequencies below 2 kHz (for plate a_1), or below 1.2 kHz (for plate a_3), it can be seen that the model accounts for the apparent erratic law of dependence of damping on frequency. For frequencies above the critical frequencies (6 kHz for a_1, 3 kHz for a_3), the asymptotic radiation model

TABLE I. Measured elastic and geometrical parameters of the plates.

Aluminum plates				
$\rho = 2660\ \mathrm{kg\,m^{-3}}$	$D_1 = 6160$ MPa	$D_4 = 8600$ MPa		
plate a_1:	$l_x = 304$ mm	$l_y = 192$ mm	$h = 2$ mm	$f_c = 6$ kHz
plate a_3:	$l_x = 419.5$ mm	$l_y = 400$ mm	$h = 4$ mm	$f_c = 3$ kHz
Glass plate				
$\rho = 2550\ \mathrm{kg\,m^{-3}}$	$D_1 = 6700$ MPa	$D_4 = 10\,270$ MPa		
plate v_1:	$l_x = 229.5$ mm	$l_y = 220.5$ mm	$h = 2$ mm	$f_c = 5.8$ kHz
Carbon plate				
$\rho = 1540\ \mathrm{kg\,m^{-3}}$	$D_1 = 8437$ MPa	$D_2 = 463$ MPa	$D_3 = 852$ MPa	$D_4 = 2267$ MPa
plate c_1:	$l_x = 399$ mm	$l_y = 200$ mm	$h = 2.2$ mm	critical zone=[3.6,11.3] kHz
Wooden plate				
$\rho = 388\ \mathrm{kg\,m^{-3}}$	$D_1 = 1013$ MPa	$D_2 = 27.5$ MPa	$D_3 = 53.7$ MPa	$D_4 = 221$ MPa
plate b_1:	$l_x = 515$ mm	$l_y = 412.5$ mm	$h = 4.8$ mm	critical zone=[2.4,10.3] kHz

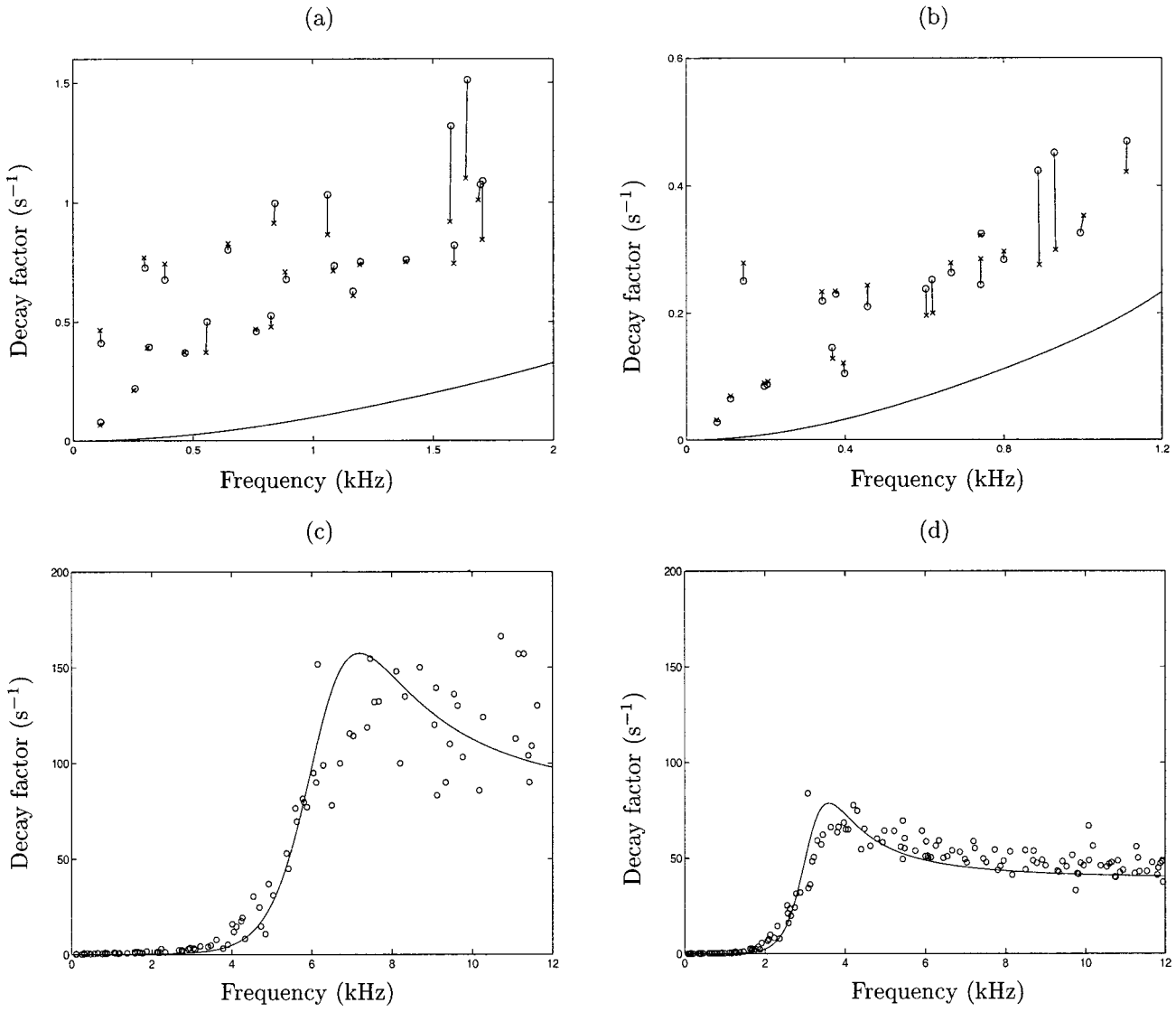

FIG. 1. Aluminum plates. Comparison between predicted and measured decay factors (in s^{-1}) vs frequency. ''○'' measured points; ''×'' predicted points with thermoelastic damping model. Solid line: asymptotic radiation model. (a) and (c) plate a_1 ($h = 2$ mm). (b) and (d) plate a_3 ($h = 4$ mm). (a) and (b) 0–2 kHz. (c) and (d) 0–12 kHz.

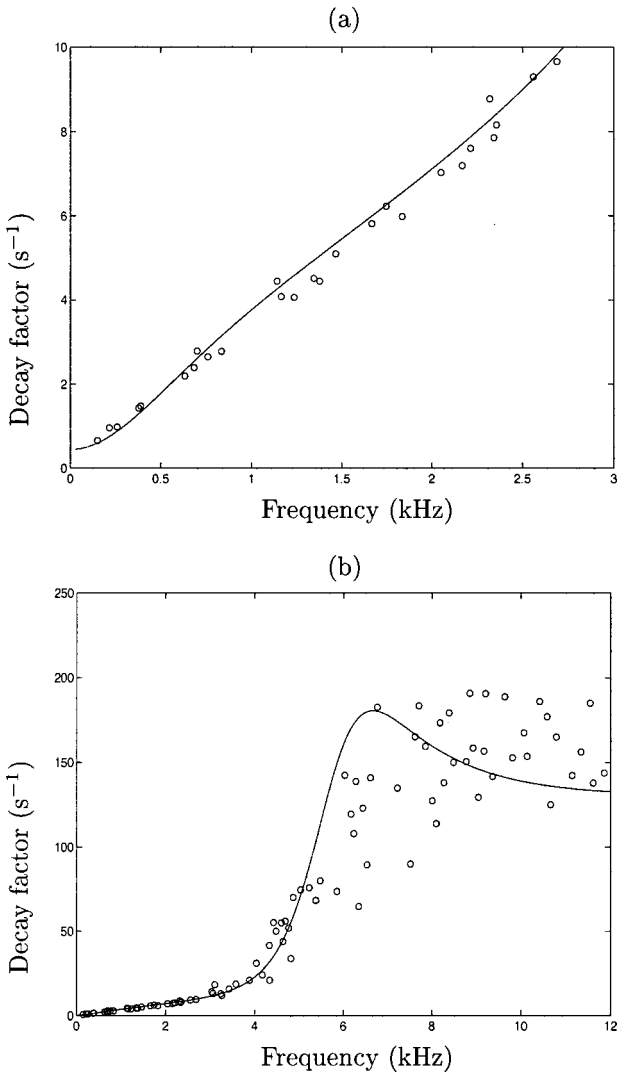

FIG. 2. Glass plate. Comparison between predicted and measured decay factors (in s^{-1}) vs frequency. (a) Solid line: viscoelastic model; ''○'' measured points. (b) Solid line: complete model (viscoelasticity+radiation); ''○'' measured points.

based on the dispersion equation for the infinite plate accounts globally for the frequency dependence of decay factors measured on finite plates. It can be seen that the standard deviation of the experimental points increases as the thickness of the plate decreases.

2. Glass

Figure 2(a) shows the decay factors measured on the rectangular glass plate for $f<3$ kHz, i.e., below its critical frequency (5.8 kHz). The results show an almost linear relationship between the decay factors and the eigenfrequencies, which completely differs from the results obtained in the case of aluminum. In addition, the decay factors are nearly ten times greater than those obtained for an aluminum plate of comparable size and thickness (plate a_1). Comparing these experimental results to Eq. (26) shows that the assumption of proportional damping is pertinent here. As a consequence, the decay factors are independent of the modal shapes of the plate. Therefore, we can write in this range:

$$\alpha_p=\frac{\omega_p}{2}\,\eta(\omega_p) \quad \text{with} \quad \eta(\omega_p)=\eta_1(\omega_p)=\eta_4(\omega_p). \tag{40}$$

Above the critical frequency [see Fig. 2(b)], the measured decay factors for the glass plate are comparable to those of the aluminum plate. Here again, the asymptotic radiation model fits well with the average value of the experimental points: a noticeable increase around the critical frequency followed by an almost constant value ($150\,s^{-1}$). The standard deviation in this range is of the same order of magnitude as that observed for aluminum plate a_1.

Below the critical frequency, the damping model for the glass plate is built with a two-cell viscoelastic model which ensures that the loss factors η_1 and η_4 are almost constant below the critical frequency:

$$\tilde{d}_{iv}(s)=\tilde{d}_v(s)=\frac{sR_1}{s+s_1}+\frac{sR_2}{s+s_2}, \quad i=1,4. \tag{41}$$

The efficiency of this viscoelastic model is shown in Fig. 2(a). The decay factors are reproduced within less than 5%. Above the critical frequency, the radiation is modeled with the perturbation term $\tilde{d}_r(s)$ given by Eq. (22). Finally, a viscous damping R_f is added, as with aluminum plates, in order to account for the damping near the zero frequency. As for the aluminum plates, it is assumed that the two mechanisms of damping are uncorrelated, and that the two perturbation terms, viscoelasticity and radiation, are added in the complex rigidities. In summary, the decay factors predicted by the model used for the glass plate are given by:

$$\alpha_p=\frac{\omega_p}{2}\,\Im m(\tilde{d}_v(j\omega_p)+\tilde{d}_r(j\omega_p))+\frac{R_f}{2}. \tag{42}$$

3. Carbon fibers

The rectangular plate made of carbon fibers used for the measurements is orthotropic, with axes of symmetry parallel to the edges. For this plate, measurements of eigenfrequencies and decay rates, used for the estimation of the damping constants and reported here, are limited to the range [0,2] kHz. The reason is that this material is highly dissipative, compared to glass and aluminum, for example. As a consequence, the bending vibrations are damped very rapidly and it is difficult to measure the decay times above 2 kHz with great accuracy. In order to allow comparisons with previous studies on such materials, the results are presented here in terms of quality factors. Figure 3 shows the dependence of quality factors on frequency for the carbon plate. The majority of the modes exhibit constant Q values around 250, although a substantial number of modes show an apparent erratic distribution of Q values, as it was the case for the aluminum plates below the critical frequency. Due to low thermal conductivity, the thermoelastic losses are negligible in such a material, and it is reasonable to assume here that the internal losses are almost entirely due to viscoelasticity.

With the assumption of a proportional damping, it was not possible here to predict the decay factors with sufficient accuracy. Therefore, in order to account for the measured decay factors, it is assumed here that the complex rigidities $\tilde{D}_i$ take the form:

$$\tilde{d}_{iv}(s)=\frac{sR_{1i}}{s+s_{1i}}+\frac{sR_{2i}}{s+s_{2i}},\quad i=(1,3,4)\ \text{ and }\ d_{2v}(s)=0, \tag{43}$$

where three of the four rigidities are perturbed by a specific two-cell viscoelastic function. As for the other materials, a viscous damping is added to the bending wave equation. Thus, the predicted decay factors are given by:

$$\alpha_p(\omega_p)=\frac{\omega_p}{2}\Im m(\tilde{d}_{1v}(j\omega_p)J_{1,p}+\tilde{d}_{3v}(j\omega_p)J_{3,p}+\tilde{d}_{4v}(j\omega_p)J_{4,p})+\frac{R_f}{2}. \tag{44}$$

Since D_2, and thus $J_{2,p}$, are relatively small compared to the other terms in Eq. (44), there is no need for adding a perturbation term to D_2, since it has no influence on the decay factors. In terms of quality factors, Eq. (44) becomes:

$$Q_p=\pi\frac{f_p}{\alpha_p}. \tag{45}$$

Unlike isotropic materials, it was not possible to derive a satisfactory approximation for the radiation damping of orthotropic plates, because of the angular dependence of the dispersion equation (see Sec. II). In some fortunate cases, the material and the geometry of the plate are such that the radiation damping is masked by other mechanisms and can be neglected. This is the case, in our study, for the carbon plate and, to a lesser extent, for the wooden plate. Otherwise, we must content ourselves with a simplified approach to the radiation modeling for orthotropic plates by considering two limiting cases: a wave traveling either in the x or in the y direction. In these cases, an upper bound f_{c3} and a lower bound f_{c1} for the critical frequency can be found by replacing D in Eq. (21) by D_3 and D_1, respectively. This yields the limits of a ''critical zone.'' Using Eq. (22), one can then derive two asymptotic curves for predicting the contribution of radiation damping in the decay factors following a procedure similar to the isotropic case. For the carbon plate under study c_1 (see Table I), for example, this zone is given by the interval [3.6,11.3] kHz. This means qualitatively that the radiation losses are higher for the eigenmodes that are spatially oriented along the x-axis.

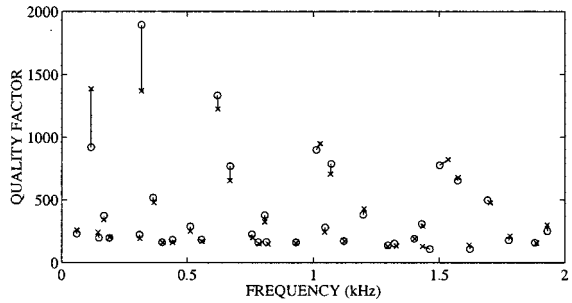

FIG. 3. Carbon plate. Comparison between predicted and measured quality factors vs frequency. ''○'' measured points; ''×'' predicted points with viscoelastic damping model. The solid lines indicate the distance between measured and predicted values.

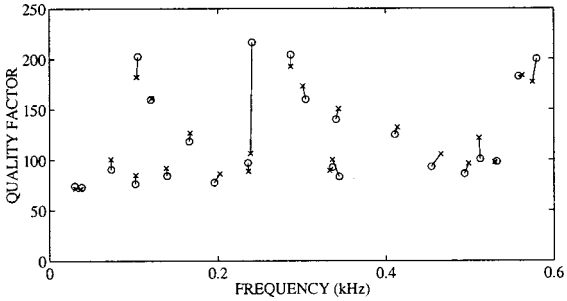

FIG. 4. Wooden plate (Spruce). Comparison between predicted and measured quality factors vs frequency. ''○'' measured points; ''×'' predicted points with viscoelastic damping model. The solid lines indicate the distance between measured and predicted values.

Figure 3 shows the comparison between measured and calculated quality factors for plate c_1 using Eq. (44), which amounts to assuming that the damping is only due to viscoelasticity. It can be seen that the model is able to predict most of the quality factors with great accuracy in the interval [0,2] kHz, except for a limited number of low-frequency modes with high Q.

4. Wood (Spruce)

The fourth measured plate b_1 is made of Spruce. This rectangular plate is cut along the Longitudinal-Radial plane (LR plane or quarter-cut).[23] This plate was selected and prepared by an instrument maker for designing a guitar soundboard. Compared to the other measured orthotropic plate in carbon c_1, the wooden plate exhibits a more pronounced degree of orthotropy $D_3/D_1\simeq 20$ (see Table I). A modal analysis performed on this plate showed some distinct asymmetry of some modal shapes which might be the consequence of heterogeneities in the material. Measurements of the thickness at different points of the plate showed relative differences of nearly 5% which also contributes to the inhomogeneous properties of the plate.

The flexural vibrations in the material are damped very rapidly, which is immediately perceptible by tapping the plate with the finger, as an instrument maker usually does for testing them. Due to the small decay times, measurements were only possible below 3 kHz. Accurate measurements were obtained for the first 23 eigenfrequencies (see Fig. 4). These measurements were used for estimating the elastic and damping constants (see Tables I and II).

For this plate, the structure of the viscoelastic model is the same as the one given in Eq. (43) for the carbon plate c_1. Consequently, the prediction of the decay factors is governed by an equation similar to Eq. (44). As for the carbon plate, the results shown in Fig. 4 are presented in terms of Q factors, using an equation similar to Eq. (45). This figure shows that the quality factor for this material is almost constant and nearly equal to 80 for a large number of modes in the observed range, with again an apparent erratic distribution for the other modes. There is excellent agreement between measured and predicted Q values, except for one mode around 230 Hz.

Here also, the radiation damping is neglected, due to the high rate of energy dissipation in the material. However, this

TABLE II. Measured damping parameters of the plates.

Thermoelastic damping (aluminum)			
$R_1 = 8.45\times 10^{-3}$	$c_1 = 8.0\times 10^{-4}$ rad m^2 s^{-1}		
Viscoelastic damping (glass)			
$R_1 = 1.63\times 10^{-3}$	$s_1 = 5180$ rad s^{-1}	$R_2 = 1.962\times 10^{-3}$	$s_2 = 55\,100$ rad s^{-1}
Viscoelastic damping (carbon)			
$R_{11} = 1.32\times 10^{-3}$	$s_{11} = 10.1\times 10^{3}$ rad s^{-1}	$R_{12} = 5.0\times 10^{-3}$	$s_{12} = 94.0\times 10^{3}$ rad s^{-1}
$R_{31} = 8.8\times 10^{-3}$	$s_{31} = 2.5\times 10^{3}$ rad s^{-1}	$R_{32} = 44.0\times 10^{-3}$	$s_{32} = 70.0$ rad s^{-1}
$R_{41} = 10.4\times 10^{-3}$	$s_{41} = 2.27\times 10^{3}$ rad s^{-1}	$R_{42} = 14.4\times 10^{-3}$	$s_{42} = 40.0\times 10^{3}$ rad s^{-1}
Viscoelastic damping (wood)			
$R_{11} = 8.18\times 10^{-3}$	$s_{11} = 3.2\times 10^{3}$ rad s^{-1}	$R_{12} = 10.0\times 10^{-3}$	$s_{12} = 50.2\times 10^{3}$ rad s^{-1}
$R_{31} = 16.7\times 10^{-3}$	$s_{31} = 1.1\times 10^{3}$ rad s^{-1}	$R_{32} = 70.0\times 10^{-3}$	$s_{32} = 50.2$ rad s^{-1}
$R_{41} = 15.2\times 10^{-3}$	$s_{41} = 1.75\times 10^{3}$ rad s^{-1}	$R_{42} = 35.0\times 10^{-3}$	$s_{42} = 50.2\times 10^{3}$ rad s^{-1}
Viscous damping			
aluminum $R_f = 0.032$ s^{-1}	glass $R_f = 0.88$ s^{-1}	carbon $R_f = 0.8$ s^{-1}	wood $R_f = 2.4$ s^{-1}

assumption is less justified here than for the carbon plate c_1 because of both the relatively larger size and lower density of the wooden plate. Schematically, it is found that the critical frequency for flexural waves propagating along the x-axis is here equal to 2.4 kHz, which means that the radiation damping will become significant for frequencies near and above this value. In comparison, the radiation damping for plate c_1 was found to be significant for frequencies greater than or equal to 3.6 kHz. The consequence of this is that the global damping in the model will be underestimated for frequencies above 2.4 kHz, as it will be seen in the simulations.[4] On the contrary, adding a simplified radiation contribution using an ''equivalent isotropic'' model by means of a perturbation term similar to the one shown in Eq. (22) yields an overestimation of the global damping. In the case of the present wooden plate, it has been shown that these approximations in the radiation damping do not affect substantially the estimation of the quality factors, since the radiation effects are masked by the intrinsic damping of the material.

IV. CONCLUSIONS

The aim of the work reported in this paper was to derive an appropriate model for the time-domain simulation of damped flexural vibrations in plates. The main interest of this work is to investigate the link between tone qualities and material properties by means of sound synthesis. This goal is not only of prime importance for the design of musical instruments, but also for a better understanding and control of all sources of noise, especially those resulting from impacts.

In the literature, one can find many papers dealing with the frequency domain modeling of damping in structural dynamics.[24] In comparison, relatively few papers address this problem in the time-domain. Therefore, it was decided to put emphasis here on the damping model. In musical acoustics, previous work on strings, bars, and membranes has shown the importance of accurate damping parameters in the realism of the simulated sounds.[25,26]

The strategy selected here was to take three basic mechanisms of damping in plates into account by adding perturbation terms in the rigidities. The advantage of this method is to yield a simplified system that governs the vibrations of the plate itself, without any coupling to acoustical and thermal fields. From these equations, the eigenfrequencies and decay rates of the plates can be estimated. The elastic plate model is based on the Kirchhoff–Love approximations, and is treated for a simple rectangular geometry.

The method has been validated on two isotropic (glass and aluminum) and two orthotropic (carbon fiber and wood) materials. The damping phenomena in each of these materials are, to some extent, representative of the three investigated mechanisms: thermoelasticity and radiation in aluminum, viscoelasticity and radiation in glass, viscoelasticity in carbon and wood. For each of these materials, the comparison between measured and predicted eigenfrequencies and decay factors show that the model is able to reproduce fairly well the complicated frequency dependence of the decay factors, and the influence of the plate geometry (size, thickness) on the decay times. However, the simplified asymptotic radiation model is only valid for isotropic materials and is not relevant enough for orthotropic materials. For these latter materials, it is likely that it will be necessary to model the complete fluid-structure interaction in order to predict the decay rates with sufficient accuracy, as has been done for other vibrating structures.[26]

The next step of the work will now consist of the numerical formulation of the problem in order to simulate waveforms in the time domain. In order to facilitate the future finite-difference formulation of the damped plate equations, a convenient differential operator was selected for the damping terms. Attention was paid, in particular, to the mathematical properties of this formulation, in order to ensure the well-posedness of the problem in terms of dissipativity. The numerical model and the results are presented in a companion paper.[4]

[1] T. Igarashi, M. Goto, and A. Kawasaki, ''Studies on impact sound (First report. The sound generated by a ball colliding a plate),'' Bull. JSME **28**, 148–154 (1985).
[2] T. Igarashi and T. Aimoto, ''Studies on impact sound (Second report. Mechanism of sound generation),'' Bull. JSME **28**, 1247–1254 (1985).
[3] S. Schedin, C. Lambourg, and A. Chaigne, ''Transient sound fields from impacted plates: Comparison between numerical simulations and experiments,'' J. Sound Vib. **221**, 471–490 (1999).

[4] C. Lambourg, A. Chaigne, and D. Matignon, ''Time-domain simulation of damped impacted plates. Part II. Numerical model and results,'' J. Acoust. Soc. Am. **109**, 1433–1447 (2001).
[5] A. W. Leissa, *Vibrations of Plates*, NASA SP-160 (NASA, Washington, D.C., 1969).
[6] R. F. S. Hearmon, *An Introduction to Applied Anisotropic Elasticity* (Oxford University Press, London, 1961).
[7] M. A. Biot, ''Thermoelasticity and irreversible thermodynamics,'' J. Appl. Phys. **27**, 240–253 (1956).
[8] C. Zener, ''Internal friction in solids—I. Theory of internal friction in reeds,'' Phys. Rev. **32**, 230–235 (1937).
[9] L. Cremer, M. Heckl, and E. E. Ungar, *Structure-Borne Sound*, 2nd ed. (Springer-Verlag, Berlin, 1972).
[10] R. M. Christensen, *Theory of Viscoelasticity. An Introduction* (Academic, New York, 1982).
[11] E. Skudrzyk, *Simple and Complex Vibratory Systems* (The Pennsylvania State University Press, Univeristy Park, PA, 1968).
[12] M. E. Gurtin and E. Sternberg, ''On the linear theory of viscoelasticity,'' Arch. Ration. Mech. Anal. **11**, 291–356 (1962).
[13] W. F. Ames, *Numerical Methods for Partial Differential Equations*, 3rd ed. (Academic, San Diego, 1992).
[14] D. Bonsignour, ''Caractéristiques acoustiques d'un matériau viscoélastique,'' Acustica **23**, 214–222 (1970).
[15] P. J. T. Filipi, O. Lagarrigue, and P.-O. Mattei, ''Perturbation method for sound radiation by a vibrating plate in a light fluid: Comparison with the exact solution,'' J. Sound Vib. **177**, 259–275 (1994).
[16] A. Frendi, L. Maestrello, and A. Bayliss, ''Coupling between plate vibration and acoustic radiation,'' J. Sound Vib. **177**, 207–226 (1994).
[17] G. Maidanik, ''The influence of fluid loading on the radiation from orthotropic plates,'' J. Sound Vib. **3**, 288–299 (1966).
[18] M. C. Junger and D. Feit, *Sound, Structures, and Their Interaction* (MIT Press, Cambridge, 1986).
[19] J. Laroche, ''The use of the matrix pencil method for the spectrum analysis of musical signals,'' J. Acoust. Soc. Am. **94**, 1958–1965 (1993).
[20] M. E. McIntyre and J. Woodhouse, ''On measuring the elastic and damping constants of orthotropic sheet materials,'' Acta Mech. **36**, 1397–1416 (1988).
[21] L. Meirovitch, *Analytical Methods in Vibrations* (MacMillan, New York, 1967).
[22] J. Sanchez Hubert and E. Sanchez Palencia, *Vibration and Coupling of Continuous Systems—Asymptotic Methods* (Springer-Verlag, Berlin, 1989).
[23] V. Bucur, *Acoustics of Wood* (CRC Press, Boca Raton, 1995).
[24] J. Argyris and H. P. Mlejnek, *Dynamics of Structures. Text on Computational Mechanics—Volume V* (Elsevier, Amsterdam, 1991).
[25] A. Chaigne and V. Doutaut, ''Numerical simulations of xylophones. I. Time-domain modeling of the vibrating bars,'' J. Acoust. Soc. Am. **101**, 539–557 (1996).
[26] L. Rhaouti, A. Chaigne, and P. Joly, ''Time-domain modeling and numerical simulation of a kettledrum,'' J. Acoust. Soc. Am. **105**, 3545–3562 (1999).